Investigation of the Geometry Configuration Variations on the Performance of Ion Thruster Grids with PIC-DSMC Simulations

IEPC-2015-218/ISTS-2015-b-218

Presented at Joint Conference of 30th International Symposium on Space Technology and Science, 34th International Electric Propulsion Conference and 6th Nano-satellite Symposium
Hyogo-Kobe, Japan
July 4–10, 2015

Emre Turkoz*, Firat Sik† and Murat Celik‡
Bogazici University, Istanbul, 34342, Turkey

The performance of accelerator grids is an important factor that determines the efficiency of ion thrusters. A PIC-DSMC code is developed to simulate the grid region plasma of an ion engine and to obtain optimum geometry configuration that yields the most efficient utilization of the propellant. The investigated two-grid system includes a screen and an accelerator grid, and the solution domain consists of 30^o slice of a 2 mm radius cylindrical domain with 5 mm axial length, which is the smallest representative domain of the whole grid region. The electric potentials applied on the screen and the acceleration grids result in an electric potential distribution that is obtained by solving the Poisson's equation throughout the 3D cylindrical axisymmetric domain. The motion of the ions and neutrals, that are represented by macroparticles in the system, are handled with the Leapfrog method with acceleration due to local electric potential gradient, whereas electrons are not treated as particles but handled with an analytical model. DSMC collisions are implemented for the neutral and ion species. The code is implemented using C++ programming language and the implementation benefited from multicore parallelization and the object-oriented programming capabilities. In this study, the results of the parametric study performed to find the grid configuration that yields the best performance are presented.

I. Introduction

In an ion engine, the neutral propellant is ionized inside an ionization chamber and an ion extraction mechanism is used for expelling the ions at high velocities to provide the desired thrust. Based on the ionization mechanism inside the ionization chamber, the ion thrusters are categorized as the electron-bombardment (Kaufman type) ion engines, RF (radio-frequency) ion engines, or microwave (electron-cyclotron resonance (ECR)) ion engines. A simplified schematic of an RF ion thruster is shown in Figure 1. The proper design of the ion extraction and acceleration mechanism is crucial for the performance of the ion thrusters. The subject of the ion optics studies is the investigation of the electrostatic grids that are located at the end of the discharge chamber to accelerate the ions out of the thruster to generate thrust.

At the Bogazici University Space Technologies Laboratory (BUSTLab), a prototype 80 *mm* diameter RF ion thruster, named BURFIT-80, is being built and tested. The developed PIC-DSMC model, that simulates the accelerator grid region plasma of a two grid system of an ion thruster, will be used in the ion thruster design studies including the design of the BURFIT-80 ion thruster[1] grid system. In the pursuit of building the BURFIT-80 ion thruster, a fluid model for the discharge plasma has already been developed.[2–5] With

*Currently Ph.D. Student at the Department of Mechanical and Aerospace Engineering, Princeton University, Princeton, NJ, U.S.A., emreturkoz@gmail.com.
†Undergraduate Student, Department of Mechanical Engineering, Bogazici University, Istanbul, Turkey, firats@boun.edu.tr.
‡Assistant Professor, Department of Mechanical Engineering, Bogazici University, Istanbul, Turkey, murat.celik@boun.edu.tr.

the ion optics model described in this paper, an expanded capability to model both the discharge chamber plasma and the grid region plasma of an RF ion thruster is being achieved. Parts of the developed ion optics model is described in previous works.[6,7]

A numerical model for the grid region plasma involves the evaluation of the electric field imposed by the voltage difference between the grids. In this intra-grid region, the quasi-neutrality inevitably breaks down when the ions are extracted from the discharge chamber due to the externally applied potential difference. Thus, a quasi-neutral plasma assumption cannot be made to simulate the plasma in the grid region.

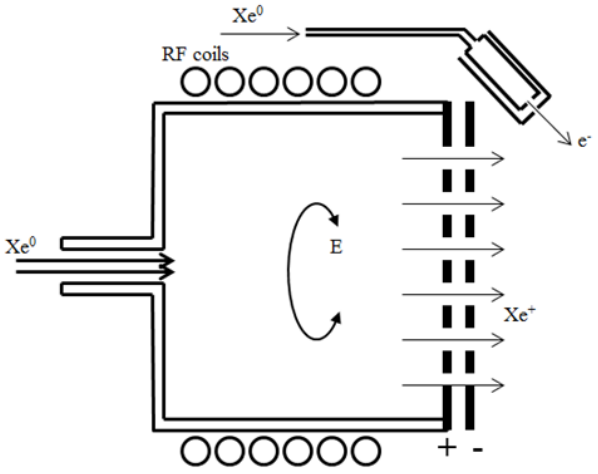

Figure 1. Schematic of an RF ion thruster

In the literature, there are several ion optics models: CEX2D[8] and CEX3D,[9] developed at Jet Propulsion Laboratory, is capable of simulating the two-grid ion optics in two dimensions and three dimensions respectively. Another ion optics model called ffx, developed by Farnell,[10] handles both particle motion and grid sputtering effects. Another model, igx,[11] employs a useful approach for simulating the hexagonal grid patterns in three dimensions which is also the approach incorporated to the work presented in this paper. The implementation of the particle model and the collision algorithm in this work is adapted from Celik's work on plasma thruster plumes.[12]

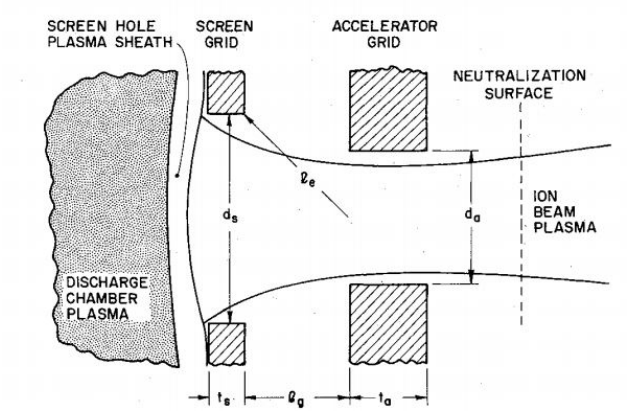

Figure 2. Schematic of a hole pair of a two-grid system[13]

In order to explain the acceleration of the ions by the electrostatic potential difference applied between two or more adjacent grids, a two-grid system, consisting of a screen and an accelerator grid, is investigated. A schematic of a hole pair of a two-grid system with a screen and an accelerator grid is shown in Figure 2.

Since ions directly affect the electric potential distribution between the grids, the ion current extraction would be restricted by the Child-Langmuir space-charge limit, and it is formulated as:

$$\mathbf{J} = \frac{4\sqrt{2}}{9}\varepsilon_0 \left(\frac{e}{m_i}\right) \frac{V_a^{3/2}}{l_g^2} \tag{1}$$

where l_g is the gap distance between the grids, V_a is the electrostatic potential difference between the grids, ε_0 is the permittivity of free space, e is the elementary charge and m_i is the mass of an ion.

If the space-charge limited current density is multiplied by the beam area, the maximum possible current can be calculated. For a beam with diameter D, the current is formulated as:

$$\mathbf{I} = \frac{\pi D^2}{4}\mathbf{J} = \frac{\pi}{4}\frac{4\sqrt{2}}{9}\varepsilon_0 \left(\frac{e}{m_i}\right) \frac{D^2}{l_g^2} V_a^{3/2} = P V_a^{3/2} \tag{2}$$

where P is called as the *perveance* of the extraction system. Taking into account the three-dimensional geometry effects, the following correction to calculate the perveance value is suggested:[13]

$$P = \frac{I_h}{V_a^{3/2}} \left(\frac{l_e}{d_s}\right) \tag{3}$$

where I_h is the beam current per hole, d_s is the screen grid aperture diameter and l_e is defined as:

$$l_e = \sqrt{l_g^2 + (d_s^2/4)} \tag{4}$$

A similar correction should be applied on the Child-Langmuir law itself to reach the correct values of the limiting current. The three-dimensional correction[14] to this law is performed by replacing the square of the gap distance, l_g^2, in Equation 1 with $(l_g + t_s)^2 + d_s^2/4$.

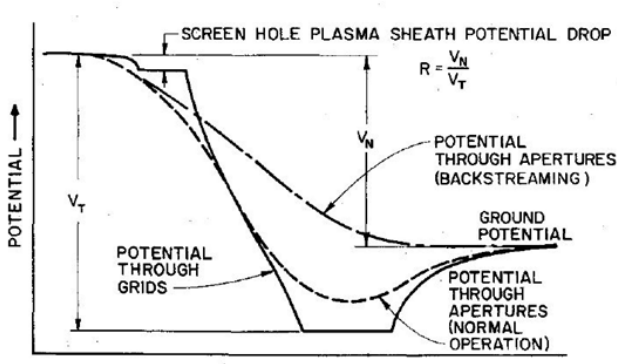

Figure 3. Potential change along a two-grid system[13]

In the design of an ion extraction system, another important factor that needs to be taken into account is the electron backstreaming phenomenon. Electron backstreaming occurs when the accelerator grid potential is so low that the grid starts to attract electrons coming out from the neutralizer cathode located outside the thruster. The level of electron backstreaming depends on the net-to-total potential ratio, $R = V_N/V_T$. Figure 3 presents an illustration of the potential through a screen-accel grid pair. As presented in this figure, V_T represents the total potential drop from discharge chamber plasma to the acceleration grid potential, and V_N represents the net potential drop between the discharge chamber plasma and the beam (or ground) potential. In Figure 3, the dashed potential line represents the potential profile in normal (no electron backstreaming) operation, whereas the dashdotted line represents the potential profile for the case of electron backstreaming.

The net-to-total potential ratio has a maximum value for the electron backstreaming not to take place. This maximum is formulated as follows:[13]

$$R_{max} = 1 - \frac{0.2}{(l_e/d_a)e^{(t_a/d_a)}} \tag{5}$$

This formula depends purely on the geometry, and proves to be a conservative estimate of the real laboratory conditions.

The numerical model, written in C++, presented in this study is a particle-in-cell (PIC) model that simulates the grid region plasma of an ion thruster. It is currently being used to analyze a two grid system, however, it is possible to modify the geometry so that three grid systems can also be investigated. Numerically, the domain is divided into cells in 3D cylindrical dimensions. The simulated macroparticles experience neutral-neutral and neutral-ion elastic collisions along with neutral-ion charge exchange (CEX) collisions that are modelled with Direct Simulation Monte Carlo (DSMC) method.

The changes in accelerator grid geometry and operation conditions result in different electric potential distributions in the intra-grid region. Therefore, the trajectory of each particle along the domain significantly changes, which may result in differences in efficiency and thrust. Thus, the aim of this work is to maximize the current leaving the domain from the downstream axial boundary by implementing optimization algorithms that provide the convergence of accelerator grids geometry to the best configuration. Besides, obtaining flatter ion trajectories - such that the ions exiting the domain have higher axial kinetic energy percentage - is another desirable design objective.

II. Ion Optics Model

In this section, a summary of the implementation details of the developed ion optics code are presented. More detailed discussions of the modules of the numerical model are presented in previous studies.[6,7] In the considered design, grids are assumed to be manufactured such that their holes are concentric with hexagons as shown in Fig. 4. A representation of the geometry where the plasma parameters are resolved in 3D is also given in the same figure. This representation form is adapted from that of *igx*[11] ion optics code.

A. Initializing Particles

Singly charged ions and neutrals are the two particle species used in this work. Each species has respective macroparticle weighting factor. The routine that is used to determine the initial positions of particles are the same for ions and neutrals. It is imposed that both of these species enter the system from the left boundary

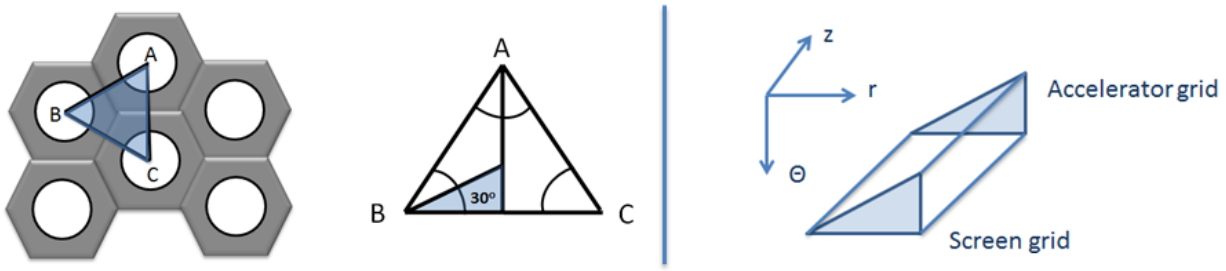

Figure 4. Ion grids geometry and the solution domain used in the model

of the domain, at the axial coordinate, $z = 0$. The radial and azimuthal coordinate locations are calculated by using two random fractions: The initial radial location, $r = r_{min} + R_1(r_{max} - r_{min})$, and the azimuthal location, $\theta = \theta_{min} + R_2(\theta_{max} - \theta_{min})$ of the particle are assigned using the random numbers R_1 and R_2.

Particle velocity initialization is performed according to the assumption that particles have Maxwellian velocity distribution. Ions entering the domain from the discharge plasma have a drift velocity, which is equal to the Bohm velocity in axial direction whereas neutrals move to the grid region without any directed velocity. But their initial velocity is always taken positive in the axial direction. The *Acceptance-Rejection Method* is used to specify the velocity for the incoming particles.[6]

After velocity components are determined for each particle in the Cartesian (x, y, z) coordinates, these components are converted into the cylindrical coordinates (r, θ, z) and stored in this way. The velocity components in Cartesian coordinates are expressed as $\mathbf{v} = v_x\hat{i} + v_y\hat{j} + v_z\hat{k}$. Their counterparts in cylindrical coordinates are: $\mathbf{v} = v_r\hat{r} + v_\theta\hat{\theta} + v_z\hat{z}$. The transformation to cylindrical coordinates is formulated as:

$$v_z = v_z \tag{6}$$

$$v_r = v_x cos(\theta) + v_y sin(\theta) \tag{7}$$

$$v_\theta = (-v_x sin(\theta) + v_y cos(\theta))/r \tag{8}$$

This transformation is performed for each particle initialized. The azimuthal velocity component is stored as rad/s. It is converted into m/s when necessary by multiplying this value with the radial coordinate of the particle.

B. Solving the Electric Potential

For the computational study, for the wedge geometry presented in Fig. 4, a structured rectangular grid is used for the sides of a 30^o angle wedge. A representative grid used in the presented analysis and an example set of boundary conditions are presented in Fig. 5.

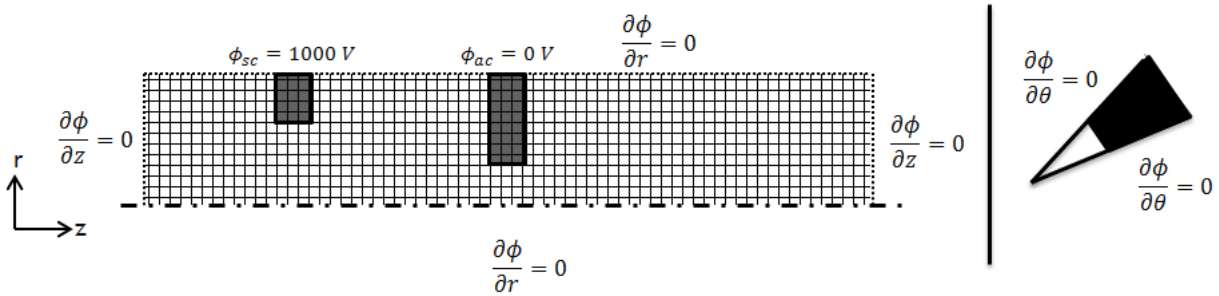

Figure 5. Solution domain: Electric potential equation is solved in 3D cylindrical coordinates on a wedge shaped domain with a 30^o angle[11]

The electric potential distribution throughout the domain is evaluated by solving the Poisson's equation:

$$\nabla^2\phi = -\frac{\rho}{\varepsilon_0} \tag{9}$$

which has the form

$$\nabla^2\phi = \frac{1}{r}\frac{\partial}{\partial r}\left(r\frac{\partial\phi}{\partial r}\right) + \frac{1}{r^2}\frac{\partial^2\phi}{\partial\theta^2} + \frac{\partial^2\phi}{\partial z^2} = -\frac{\rho}{\varepsilon_0} \tag{10}$$

in cylindrical coordinates. Here, ρ is the net charge density and ε_0 is the permittivity of free space. The charge density, is calculated by weighting each macroparticle's charge to the cell nodes. According to the weighting scheme employed in cylindrical coordinates, the accumulated charge at one node of the mesh is formulated as follows

$$\rho_n = \rho_n + \frac{q_p}{V_{cell}}\left(1 - \frac{|(z_n - z_p)\pi(r_n^2 - r_p^2)(\theta_n - \theta_p)|}{V_{cell}}\right) \tag{11}$$

where ρ_n denotes the charge density of the node, q_p is the charge that the particle is carrying in Coulombs, and z, r and θ denotes the axial, radial and azimuthal coordinates, respectively. Use of ρ_n on both sides of the equation is done to indicate that this is actually a summation over each particle which is located in a cell that harbors this node. The subscript p denotes the particle and the subscript n denotes the node considered. V_{cell} denotes the cell volume in cylindrical coordinates:

$$V_{cell} = \pi\Delta r(r_L + r_U)\Delta z\Delta\theta \tag{12}$$

where r_L is the radial position of the lower node, and r_U is the radial position of the upper node of the cell. Similarly, the weighting scheme is employed to interpolate the potential gradients calculated on the mesh nodes to the particles. This scheme is as follows:

$$(\nabla\phi)_p = (\nabla\phi)_p + (\nabla\phi)_n\left(1 - \frac{|(z_n - z_p)\pi(r_n^2 - r_p^2)(\theta_n - \theta_p)|}{V_{cell}}\right) \tag{13}$$

By utilizing the weighting scheme, the total electric field on a macro particle is calculated with the contributions coming from the 8 nodes that constitute the cell that the particle is located. To solve for the PDE for the electric potential, the second-order finite differencing scheme is applied to evaluate the coefficients. On a structured mesh, where the mesh sizes Δr, Δz, $\Delta\theta$ are equal on the grid, the finite differencing scheme for the central nodes takes the form:

$$\nabla^2\phi = \frac{\phi_{i-1,j,k} - 2\phi_{i,j,k} + \phi_{i+1,j,k}}{\Delta z^2} + \frac{\phi_{i,j-1,k} - 2\phi_{i,j,k} + \phi_{i,j+1,k}}{\Delta r^2} + \frac{\phi_{i,j,k-1} - 2\phi_{i,j,k} + \phi_{i,j,k+1}}{r^2\Delta\theta^2} + \frac{\phi_{i,j+1,k} - \phi_{i,j-1,k}}{2\Delta r} \tag{14}$$

where i denotes the node index in the axial direction, j denotes the node index in the radial direction, and k denotes the node index in the azimuthal direction.

The electric field is calculated as the gradient of the potential:

$$\mathbf{E} = -\nabla\phi = -\left(\frac{\partial\phi}{\partial r}\hat{\mathbf{r}} + \frac{1}{r}\frac{\partial\phi}{\partial\theta}\hat{\theta} + \frac{\partial\phi}{\partial z}\hat{\mathbf{z}}\right) \tag{15}$$

C. Moving the Particles

After the electric potential and the electric field are evaluated, the ions move according to the force applied on them.[6] The particle motion is performed with the commonly used Leapfrog algorithm.[15] According to this method, for each macro particle the following equations are valid:

$$\mathbf{r}_i = \mathbf{r}_{i-1} + \mathbf{v}_{i-\frac{1}{2}}\Delta t \tag{16}$$

$$\mathbf{v}_{i+\frac{1}{2}} = \mathbf{v}_{i-\frac{1}{2}} + \mathbf{a}_i\Delta t \tag{17}$$

$$\mathbf{v}_{\frac{1}{2}} = \mathbf{v}_0 + \mathbf{a}_0\frac{\Delta t}{2} \tag{18}$$

During the particle movement only the acceleration is changed at each time step. The acceleration is directly evaluated from the force applied by the electric field on the macro particles:

$$\mathbf{F} = q\left(\mathbf{v}\times\mathbf{B} + \mathbf{E}\right) = m\mathbf{a} \tag{19}$$

where the force due to the magnetic field is considered to be negligible in the vicinity of the grid. With this simplification, a macro particle's acceleration is calculated as:

$$\mathbf{a} = \frac{q}{m}\mathbf{E} \tag{20}$$

As stated above, this acceleration value is found for each particle. But the electric field is evaluated on the nodes of the cell, not on the individual particles. Therefore, a reverse weighting scheme is necessary to evaluate the electric field on each particle.

In order to obtain a correct simulation and to prevent divergence of numerical iterations, energy conservation for macro particles is applied explicitly. The particles are assumed to conserve their energy throughout the simulation domain:

$$E_{total} = \frac{1}{2}m|\mathbf{v}|^2 + q\phi \tag{21}$$

At the end of each time step, the energy of the macro particle is forced to remain constant by modifying the magnitude of the velocity vector:

$$v_{conserved} = \sqrt{\frac{2}{m}\left(E - q\phi\right)} \tag{22}$$

$$\alpha = \frac{v_{conserved}}{v} \tag{23}$$

$$v_{conserved} = \sqrt{(\alpha v_x)^2 + (\alpha v_y)^2 + (\alpha v_z)^2} \tag{24}$$

D. Collisions with the Grid Walls

Collisions with the grid walls are handled so that particles colliding with the walls are reflected back into the system with the same momentum.

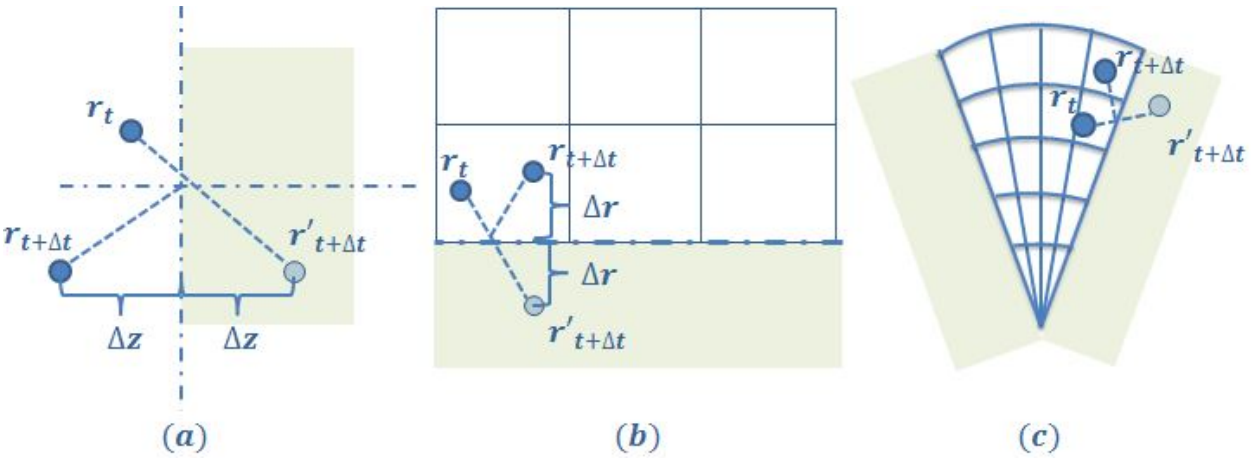

Figure 6. (a) Representation of the position change after axial reflection. (b) Representation of the position change after radial reflection from the center line. (c) Representation of the position change after azimuthal reflection

The code implemented understands that a collision with grid walls occurred during the phase where the particles are relocated and reassigned to the cells they moved in. Reflection from radial, azimuthal and the axial boundaries is performed during the relocation of each particle to its corresponding cell. There is a routine at each time step to find the cells that the particles are located in after the motion from the previous time step. During this relocation, the particles that cross the boundary are reflected back.

The axial reflection scheme is performed as represented in Figure 6a. In this figure the shaded area represents the grid wall. A particle that has the position $\mathbf{r}$ at time t is marched in time with a specific velocity and goes through a grid wall. During the particle reallocation process, the axial distance between the particle inside the grid and the grid wall is calculated. This value is shown with Δz. A calculation scheme is developed to understand whether the particle has entered from the left or right side of the grid wall. According to this scheme, the distance of the particle to the both ends of the grid is calculated.

The radial reflection is depicted in Figure 6b. Particles crossing the centerline ($r = 0$) and the top boundary ($r = r_{max}$) are handled with the simple principle that for each particle leaving the domain, there should be another one entering the domain because of the axisymmetry. The code implemented understands that a particle has crossed the centerline when its radial coordinate obtains a negative value. Similarly if a particle has a radial coordinate larger than r_{max}, the particle is reflected from the top boundary.

The azimuthal reflection is depicted in Figure 6c. The code implemented understands that a particle has crossed the boundaries by doing an *if-check* on the θ coordinate of each particle. If θ coordinate is negative or larger than θ_{max}, the reflection procedure is applied. The azimuthal coordinate of the particle after the position is updated with the velocity is denoted with $\theta'_{t+\Delta t/2}$. Particles crossing the azimuthal boundaries ($\theta = 0$ and $\theta = \theta_{max}$) are handled assuming that for each particle that crosses the boundary, there is another one that enters the domain from the same location due to the symmetry condition.

E. Collisions between Particles

Collisions between particles are handled with the conventional DSMC approach, so that particles in a particular cell collide only with the ones in that cell. In our model, elastic collisions between neutrals, elastic collisions between ions and neutrals, and charge-exchange (CEX) collisions between ions and neutrals are modeled.

The probability of a collision to occur is calculated by using the collision cross-section and collided pair's relative speed. In collision mechanics, the collision frequency is proportional to three variables. These are the densities of the collision partners, the relative velocity of the colliding particles and the collision cross section. The collision frequency of a particle colliding with another one can be formulated as:

$$\nu = n c_r \sigma \tag{25}$$

where n denotes the effective number density, c_r is the relative speed, and σ is the collision cross section.The term σc_r has the units $[m^3/s]$ and denotes the volume swept out by the particle per second for the considered collision type. In our model, the number density, and the relative velocity multiplied with collision cross section are separated from each other during the handling of collisions.

Collisions are handled using the Cartesian coordinate system, therefore the velocity components are converted first from cylindrical into Cartesian coordinate system, thus from (v_r, v_θ, v_z) to (v_x, v_y, v_z). After the collision process takes place, the resulting post-collision velocities are then converted back to cylindrical coordinates and assigned to respective collided macroparticles. Details of the collision algorithm are presented in a previous work.[6]

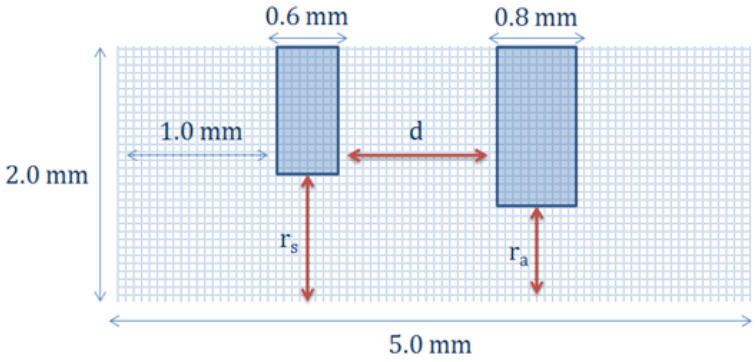

Figure 7. Dimensions of the solution domain for simulations

III. Results and Discussions

The domain investigated within the scope of this work is depicted in Figure 7. The solution domain is divided into 62 x 62 x 10 nodes, which are in axial, radial and azimuthal directions, respectively. The solution domain parameters (domain lengths, grid thicknesses, etc.) and voltages are adapted from the work

of Farnell.[10] The applied voltages are 2241 V and -400 V for the screen and acceleration grids, respectively. The upstream discharge plasma potential (left wall) is assumed to be 25 V above the screen grid potential, whereas the plume region (right wall) potential is set to 0 V.

The radial current distribution of the ions exiting the grid system is an important parameter in the ion grid system design. Preventing the ions from hitting the grid walls is one of the goals of the grid design. One of the utilities of the presented PIC-DSMC code is the ability to track particles along their short journey within the solution domain. Randomly selected particles are tracked by recording their radial and axial coordinates at each time-step. The azimuthal coordinates are not taken into account because of the axisymmetry assumption in azimuthal direction. Some of the obtained trajectories are depicted in Figure 8.

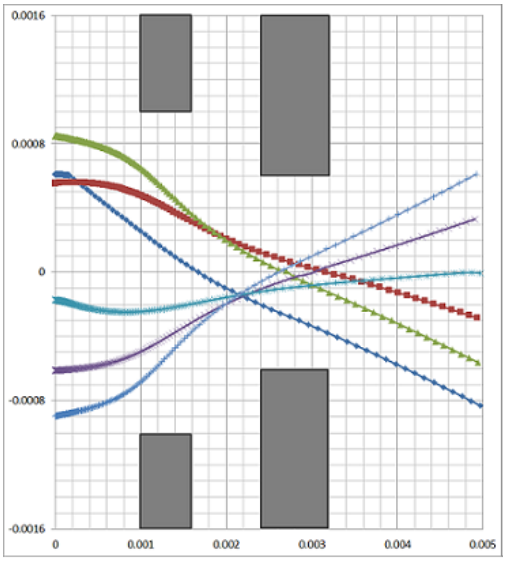

Figure 8. Trajectories of several of the ion macro particles along their motion within the computational domain

The purpose of the current study is to determine the capabilities of the developed code to vary the geometry and to find the optimum geometrical configuration for the highest current extracted. The grid thicknesses and the distance of the screen grid to the upstream boundary are kept constant. The geometrical parameters that were varied are the distance between the two grids, d, the radius of the screen grid hole, r_s, and the radius of the accel grid hole, r_a. Figures 9 presents the variation in the beamlet current for varying accel grid radius, screen grid radius and grid distance, respectively.

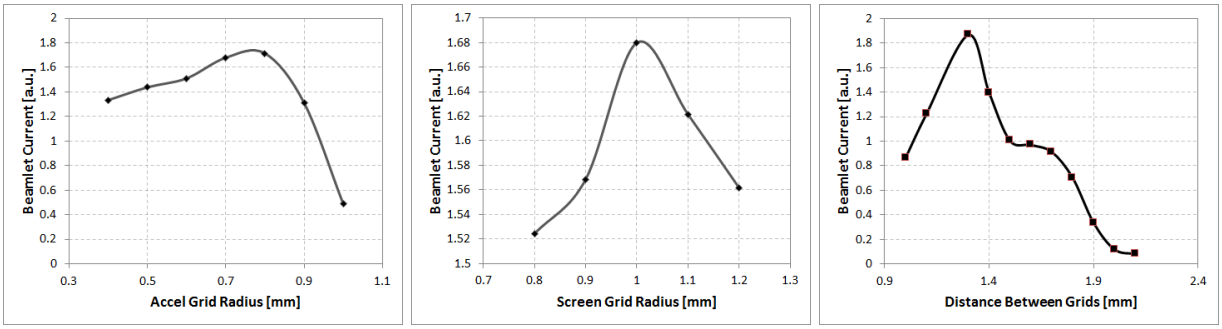

Figure 9. Change in the beamlet current for a) varying accel grid radius (for d =1.8 mm and r_s=1 mm), b) varying screen grid radius (for d =1.3 mm and r_a=0.6 mm), c) varying grid distance (for r_a=0.8 mm and r_s=1.0 mm)

IV. Conclusion

A particle-in-cell plasma simulation model to be used in the design of ion thruster grid systems is developed. The developed model uses axisymmetric cylindrical coordinates in three-dimensions. The solution domain is chosen so that it represents the smallest symmetric section of a two-grid system. The code is implemented using the C++ programming language and uses the object oriented programming. DSMC collision algorithm is implemented to simulate the collisions between the heavy particle species.

In order to find the grid parameters that maximize the beamlet current leaving the domain from the downstream axial boundary, a parametric study is conducted for the accel grid hole radius, decel grid hole radius and the grid separation distance. The results are presented.

Acknowledgment

This work was supported in part by The Scientific and Technological Research Council of Turkey under projects TUBITAK-112M862 and TUBITAK-113M244 and in part by Bogazici University Scientific Research Projects Support Fund under projects BAP-6184 and BAP-8960.

References

[1]Yavuz, B., Turkoz, E., and Celik, M., "Prototype design and manufacturing method of an 8 cm diameter RF ion thruster," *6th International Conference on Recent Advances in Space Technologies (RAST)*, IEEE, 2013, pp. 619–624.

[2]Turkoz, E. and Celik, M., "2D Fluid Model for Axisymmetric RF Ion Thruster Cylindrical Discharge Chamber," 49^{th} *Joint Propulsion Conference*, San Jose, CA, July 2013, also AIAA-2013-4110.

[3]Turkoz, E. and Celik, M., "2D Axisymmetric Fluid and Electromagnetic Models for Inductively Coupled Plasma (ICP) in RF Ion Thrusters," 33^{rd} *International Electric Propulsion Conference*, Washington DC, USA, October 2013, also IEPC-2013-294.

[4]Turkoz, E. and Celik, M., "2D Electromagnetic and Fluid Models for Inductively Coupled Plasma for RF Ion Thruster Performance Evaluation," *IEEE Transactions on Plasma Science*, Vol. 42, No. 1, Jan 2014, pp. 235–240.

[5]Turkoz, E. and Celik, M., "AETHER: A simulation platform for inductively coupled plasma," *Journal of Computational Physics*, Vol. 286, 2015, pp. 87–102.

[6]Turkoz, E., Sik, F., and Celik, M., "A Study of Ion Thruster Optics through Particle Simulations and Evaluation of the Near Plume Plasma Properties," 50^{th} *Joint Propulsion Conference*, Cleveland, OH, July 2014, also AIAA-2014-3412.

[7]Turkoz, E., Sik, F., and Celik, M., "Trajectory Studies through Numerical Simulation of Ion Thruster Grid Region Plasma with PIC-DSMC Approach in 3D," 5^{th} *Russian-German Conference on Electric Propulsion*, Dresden, Germany, September 2014.

[8]Brophy, J. R., Katz, I., Polk, J. E., and Anderson, J. R., "Numerical simulations of ion thruster accelerator grid erosion," *AIAA Paper*, Vol. 4261, 2002, pp. 2002.

[9]Anderson, J. R., Katz, I., and Goebel, D., *Numerical simulation of two-grid ion optics using a 3D code*, Pasadena, CA: Jet Propulsion Laboratory, National Aeronautics and Space Administration, 2004.

[10]Farnell, C., "Performance and Lifetime Simulation of Ion Thruster Optics," Ph.D. Dissertation, Colorado State University, Fort Collins, CO, USA, 2007.

[11]Nakayama, Y. and Wilbur, P. J., "Numerical Simulation of High Specific Impulse Ion Thruster Optics," *27th International Electric Propulsion Conference*, Pasadena, CA, 2001, also IEPC-01-099.

[12]Celik, M., Santi, M. M., Cheng, S. Y., Martinez-Sanchez, M., and Peraire, J., "Hybrid-PIC Simulation of a Hall Thruster Plume on an Unstructured Grid with DSMC Collisions," 28^{th} *International Electric Propulsion Conference*, Toulouse, France, March 2003, also IEPC–03–134.

[13]Rovang, D. C. and Wilbur, P., "Ion Extraction Capabilities of Two-Grid Accelerator Systems," *Journal of Propulsion and Power*, Vol. 1, No. 3, 1985, pp. 172–179.

[14]Wilbur, P. J., Beattie, J. R., and Hyman, J., "Approach to the parametric design of ion thrusters," *Journal of Propulsion and Power*, Vol. 6, No. 5, 1990, pp. 575–583.

[15]Fox, J. M., "Advances in Fully-Kinetic PIC Simulations of a Near Vacuum Hall Thruster and Other Plasma Systems," Ph.D. Thesis, Massachusetts Institute of Technology, Cambridge, USA, 2007.